How increasing pressure affects the ion hydration structure and shell properties at ambient temperature

Luca Tonti[a], Franca Maria Floris[b,]

[a] *Department of Chemical Engineering and Analytical Science, The University of Manchester, The Mill, Manchester M1 3AL, United Kingdom*
[b] *Dipartimento di Chimica e Chimica Industriale, Università di Pisa, Via Giuseppe Moruzzi 13, 56124 Pisa, Italy*

Abstract

This work deals with the effect of increasing pressure at 298.15 K on the structure and hydration shell properties of ions in infinitely diluted solutions. Results were obtained from NPT Monte Carlo simulations at various pressures, from 1 atm up to 8000 atm, for some alkali metal, alkaline earth and halide ions in TIP4P water. As pressure increases, the ion-O and the ion-H radial distribution functions (rdfs) are subjected to changes to differing extents depending on both the charge and the size of the ion. The first peak of the ion-O rdf is shifted to a shorter distance from the ion for Cs^+, Br^- and I^-, while in the other cases there is no evidence of shortening. In contrast, for the alkaline earth ions, the most prominent effect is the decrease in the height of the first peak. Minima positions of the ion-O rdfs were used to define the first and the second hydration shells at a given pressure. Water dipole orientation with respect to the radial direction was examined, show-

Email addresses: lucatonti@postgrad.manchester.ac.uk (Luca Tonti), floris@dcci.unipi.it (Franca Maria Floris)

ing that at higher pressures the ion-dipole interaction becomes less attractive than at 1 atm. A much less favourable orientation was found for waters in the first shell of halide ions. Shell properties were computed from definite integrals of the ion-O rdfs, such as the coordination number and the shell contribution to the excess volume. For the first hydration shell, apart from Ca^{2+}, there is a significant increase in the coordination number upon increasing pressure. This effect becomes more important the larger the ion size is and this is very significant for alkali metal and halide ions. In the case of I^{-} the gap observed between 4 katm and 5 katm reflects the striking effect of increasing pressure on the shell definition. The coordination number remains almost constant when using an alternative boundary for the shell. This was suggested by the radial distribution of water-dipole orientations. Shell excess volume contributions are discussed by examining their dependence on pressure. Electrostriction is shown for the first shell, while the second shell's contribution to the excess volume is positive. At a higher pressure, the shell electrostrictive volume per water molecule is always less than at 1 atm. The greatest effect is shown for the first shell of alkaline earth. The effect of a different shell boundary is examined on the shell quantities of halide ions.

Keywords:

high pressure, ion hydration, simulations, electrostrictive volume, shell excess volume, dipole orientation

---

1. Introduction

From studies mainly at ambient conditions, ions in water have been characterized as "structure making" or as "structure breaking" [1]. On the one hand, it is recognised that the strong field of an ion yields structural changes in the first hydration shell, due to specific orientations of waters with respect to the ion and electrostriction [2]. On the other hand, Marcus pointed out that the distinction should be made on the basis of the extent of hydrogen bonding around the ion, even beyond the hydration shells. Following Marcus [1], several anions, including halide ions, are classified as "breaking", but also some cations, such as the alkali metal ions, belong to the same class, even if at a lower level than the halide ions. According to the same classification, cations with a higher charge are generally "making" such as some molecular anions. Different series have been compiled and the relative position of two ions can also be reversed depending on the conditions of the experiments. However, ion specificity has been noted in lists based on partial molar volumes and electrostriction determined in protic and aprotic solvents [3]. Regarding ions dissolved in water, this specificity is explained in terms of the charge and the size of the ion, on which the level of hydration depends. These features can be generally correlated to the concept of a "making" or a "breaking" structure. A small ion with a high charge produces strong hydration and is generally considered to be "structure making", while a large ion with a low charge is to be often related to weak hydration and is considered to be "structure breaking".

Water structure depends also on pressure and temperature either in pure liquid or in solutions [4]. The interest in different conditions spans from

physical chemistry, biochemistry to technological applications. A specific interest has been devoted to the denaturation of proteins under increasing pressure [5, 6, 7], which has stimulated studies on how the solvation of hydrophobic and polar solutes is affected by different conditions [5, 4, 8, 9]. In contrast, there is a limited number of works concerning this kind of study on ions dissolved in water [10, 11, 12, 4, 13]. Such systems are of fundamental importance, also because ions are usually present in biological systems [14].

The aim of this work is to investigate how hydration shells around an ion are affected by the increase in pressure at isothermal conditions (298.15 K). Detailed information on structure is provided by classic NPT Monte Carlo results for single monoatomic ions of different charge and size, chosen among the alkali metal, alkaline earth and halide ions. To be consistent with the previous works on cavities [15, 9], we have inserted ions in TIP4P [16] water. This choice offers the right compromise between a moderate cost of simulations and a reasonably realistic description of water properties along the isotherm. Other details of simulations are given in section 2.1. The hydration structure is studied using the radial distribution functions (rdfs), which have been integrated in order to obtain the coordination number and shell contributions to the excess volume (section 2.2). Furthermore, we study water orientation with respect to the ion (section 2.3). Results are presented and discussed in section 3. Finally, the main conclusions are drawn in section 4, where we give some ordering of the ions on the basis of shell properties.

2. Calculation

2.1. Simulations

Classic Monte Carlo simulations were performed on a constant number of particles and at constant temperature and pressure (NPT) by using the BOSS program [17]. All the systems were composed of 512 TIP4P [16] water molecules and one atomic ion at a fixed position in the center of a cubic box with periodic boundary conditions (PBC). The molar fraction of the ion with this setup was therefore less than 0.002. Systems were studied at various pressures (1, 1000, 2000, 3000, 4000, 5000, 6000, 7000, 8000 atm) while temperature was fixed at 298.15 K in all cases. The ion-water interaction potentials contained in the OPLSAA force field were used. These are the ones published by Jensen and Jorgensen [18] for alkali (K^+, Rb^+, Cs^+) and halide ions (I^- and Br^-), and by Åqvist [19] for alkaline earth ions (Ca^{2+},Sr^{2+},Ba^{2+}). We note that their parametrization was based on free energy calculation by FEP using spherical boundary conditions and that their transferability to the PBC setup was tested [18]. Moreover, the TIP4P model was parameterized using PBC without Ewald summation [16]. The same conditions were adopted in our simulations as this choice appeared convenient and consistent. The cutoff radius for ion-water and water-water interactions was set at 11.5 Å, which was the closest to and yet lower than half of the length of the box for the Ca^{2+}-water system at 8000 atm, the system with the smallest volume.

Equilibrated water with cavities [15, 9] of appropriate size at the pressures investigated were used as initial configurations. Simulations of 50M configurations were performed in order to equilibrate the systems. Averages were

computed using 650M configurations, which were divided into 2M blocks in order to compute standard errors.

2.2. Shell properties from rdfs

Definite integrals involving $ion - O$ rdfs are used to compute shell coordination numbers and shell hydration contribution to the excess volume for an infinitely dilute solution. For a spherical solute (M), the average number of water oxygens (O) in the spherical volume of radius R centered on M is

$$n(R) = \rho \int_0^R g_{MO}^{NPT}(r)(4\pi r^2)dr, \tag{1}$$

where we have specified that, in this work, simulation rdfs were computed in the NPT ensemble and ρ is the water number density. The corresponding coordination number in the first hydration shell is defined as

$$cn_I = n(r_1) \tag{2}$$

and in the second shell as

$$cn_{II} = n(r_2) - n(r_1), \tag{3}$$

r_1 and r_2 being the $ion - O$ distances used to the define the shells.

According to the Kirkwood-Buff (KB) theory [20] applied to a spherical solute in an infinitely diluted aqueous solution, the excess volume can be computed from the KB integral

$$v_s^* = -\int_0^\infty [g_{MO}^{\mu VT}(r) - 1](4\pi r^2)dr. \tag{4}$$

The shell contribution to this quantity can be introduced as the definite integral between the distances used to define the shell [21]. In this work, for the first shell

$$\Delta V_{shell_I} = -\int_{r0}^{r1} [g_{MO}^{\mu VT}(r) - 1](4\pi r^2)dr \tag{5}$$

with r_0 defining the spherical volume around the solute from which oxygen centers are excluded. Apart from a hard-sphere solute, there could be some arbitrariness in the definition of this radius. In this work, r_0 has been defined as the shortest $ion - O$ distance at which g(r) assumes a value different from zero. The second shell contribution to the excess volume can be obtained by the integral of the same quantity between r_1 and r_2, namely

$$\Delta V_{shell_{II}} = -\int_{r1}^{r2} [g_{MO}^{\mu VT}(r) - 1](4\pi r^2)dr. \tag{6}$$

The excess volume can be written in terms of these contributions,

$$v_s^* = V_0 + \Delta V_{shell_I} + \Delta V_{shell_{II}} + other\ terms \tag{7}$$

where V_0 is the spherical volume of radius r_0. Clearly, eqs. 2, 3, 5 and 6 define shell quantities relative to r_1 and r_2, whose value can be fixed according to the shell definition chosen. The values fixed to the first two minima of g (r) correspond to the most common choice.

The Kirkwood-Buff theory of solutions was formulated within the grand canonical ensemble and the g(r) in Eqs. 4, 5 and 6 should be consistently determined as specified by the notation used above. However, in the literature KB integrals have been computed using g(r) determined at NPT conditions, usually introducing a renormalization factor [22, 15]. In this work we use the ratio $N/(< V > \rho_0)$, with N the number of water molecules in the box,

$< V >$ the average volume of the simulated system and ρ_0 the number density of TIP4P water obtained from previous simulations [15, 9]. Then, the shell contributions to the excess volume can be rewritten as the sum of two terms,

$$\Delta V_{shell_I} = -\frac{cn_I}{\rho_0} + \frac{4\pi(r_1^3 - r_0^3)}{3} \tag{8}$$

and

$$\Delta V_{shell_{II}} = -\frac{cn_{II}}{\rho_0} + \frac{4\pi(r_2^3 - r_1^3)}{3} \tag{9}$$

where the second term in the equations above represents the spherical shell volume where oxygens of waters belonging to the shell are found. We computed also the corresponding quantities normalized to the number of water oxygens in the shells, $\delta\Delta V_I = \Delta V_{shell_I}/cn_I$ and $\delta\Delta V_{II} = \Delta V_{shell_{II}}/cn_{II}$. We recall that these normalized quantities express the difference between the inverse of an averaged local number density and $1/\rho_0$.

2.3. The water dipole orientation in the hydration shells of monoatomic ions

In this work, the water orientation with respect to the ion is studied by examining α, the angle between the $ion - O$ vector distance and the vector from the oxygen towards the hydrogen centres oriented along the C_2 axis of the water molecule. Since in TIP4P water the negative charge is positioned on the same axis, the angle α defines the ion-dipole orientation.

We present results for $\langle\alpha\rangle$ obtained averaging the angle on waters belonging to the first hydration shell. Local minima positions of the $ion - O$ rdf were used to define the extent of the first two hydration shells. Hence, a water molecule belongs to the first hydration shell if the corresponding $ion - O$

distance is less than r_1. Results of the angle averaged on waters of the second shell are not presented here, while we have preferred to provide a more detailed information on dipole orientation in the first shell and beyond. To this aim, the radial distribution of $\langle cos\,(\alpha)\rangle_r$ was computed by averaging the cosine values on water molecules whose oxygens were at a distance between $r - 0.05\mathring{A}$ and $r + 0.05\mathring{A}$ from the atomic ion.

Both quantities, $\langle\alpha\rangle$ and $\langle cos\,(\alpha)\rangle_r$, were computed in post-processing from saved configurations. One configuration every 25K simulated was saved, for a total of 80 per block and 26K configurations for the entire simulation.

3. Results and discussion

3.1. Ion hydration at ambient conditions

In order to test the setup of our simulations, we first compare the results obtained at ambient conditions with experimental [23, 1] and simulation results [19, 23, 24, 18, 1] from the literature. Tables 1-3 provide this comparison for the first maximum position of $ion - O$ rdfs, the coordination number and the angle between the $ion - O$ direction and the water dipole in the first shell.

For alkali metal and halide ions it is worthwhile comparing our results with those of Jensen and Jorgensen [18], which were obtained with a large spherical drop. Since exactly the same model potentials were used, TIP4P [16] for water and for the ions the new LJ parameters optimized by Jensen and Jorgensen, discrepancies in the simulation results might arise from the different boundary conditions. However, even if our results show systematic overestimation with respect to their best results, in the worst cases these are

Table 1: First maximum position (Å) of the ion-O rdfs obtained from NPT Monte Carlo simulations of the ions (OPLSAA parameters) in a box containing 512 TIP4P waters at 298.15 K and 1 atm. Comparison of our results with those obtained by Jensen and Jorgensen [18] and with simulation and experimental results from the literature.

	$this\ work^a$	$ref(18)^b$	$other\ works^c$
K^+	2.88	2.85	2.65-2.81
Rb^+	3.02	2.95	2.90
Cs^+	3.21	3.20	3.20
Ca^{2+}	2.41	/	2.40-2.50
Sr^{2+}	2.61	/	2.57-2.63
Ba^{2+}	2.79	/	2.81
Br^-	3.39	3.35	3.32
I^-	3.62	3.55	3.63-4.22

[a] Statistical uncertaintes of 0.01

[b] See Reference [18]; statistical uncertaintes of 0.025

[c] See Reference [1]

of only 0.07 Å(Rb^+ and I^-) for the position of the first peak of the $ion-O$ rdf (see Table 1) and of $0.6-0.7$ (Rb^+ and Cs^+) for the coordination number (see Table 2). Such discrepancies are respectively within three and two times statistical uncertainties [18] and should considered to be small.

Also for the alkaline earth metal ions the comparison with Åqvist's results [19] refers to the same LJ parameters and different boundary conditions, although in this case the SPC model was used for water. Results show a very good agreement, with the first peak position overestimated by only

Table 2: The coordination number in the first hydration shell of the ions at 298.15 K and 1 atm. Comparison between our results with those obtained by Jensen and Jorgensen [18] and with simulation and experimental results from the literature.

	cn_I		
	$this\ work^a$	$ref(18)^b$	$other\ works^c$
K^+	7.3	7.0	6-8.3
Rb^+	7.8	7.2	6-8.9
Cs^+	8.6	7.9	8-9.2
Ca^{2+}	8.0	/	7-8.6
Sr^{2+}	8.8	/	8-8.1
Ba^{2+}	9.2	/	8.1
Br^-	7.8	7.7	8
I^-	8.4	7.9	7.6-8

[a] Statistical uncertaintes of around 0.1, including the uncertainty in reading the minimum position of the rdf. These uncertainties were estimated from integrals of $g(r) \pm \sigma$ and are larger then those obtained on the basis of error propagation on the integral.

[b] See Reference [18]

[c] See Reference [1]

0.03 Å in the worst case (Sr^{2+}).

Overall, PBC do not affect the definition of hydration shells and a box of 512 waters can be considered sufficiently large for the purpose of this work. On the contrary, these results can depend much more on the model potential used to describe ion-water interactions. For example, the first peak position computed for $Ca^{2+} - O$ is underestimated by 0.1 Å and the coordination

Table 3: The average of the ion-water dipole angle (α) in the first hydration shell of the ions at 298.15 K and 1 atm. Comparison between our simulation results and literature data.

	$\langle\alpha\rangle$	
	this work	*other works*
K^+	50.3(2)	20-55[a]
Rb^+	52.8(1)	59[b]
Cs^+	56.2(1)	50.2-57[a]
Ca^{2+}	22.4(1)	26-51[a]
Sr^{2+}	25.0(1)	/
Ba^{2+}	26.8(2)	/
Br^-	125.7(1)	/
I^-	123.9(1)	/

[a] See Reference [23]

[b] See Reference [25]

number by 0.6 with respect to simulation results of Floris et al. [24].

Regarding comparison with experimental results, the fact that they fall within a larger range than the one we obtained can be related to the different concentration of the ion and the presence of the counterion [23, 1]. This holds also when comparing the angle which defines water dipole orientation with respect to the ion (Table 3)).

3.2. The effect of increasing P on ion-water rdfs

The water structure around ions strongly depends on the strength of the ion field and on the sign of the charge. This is depicted in the $ion - O$

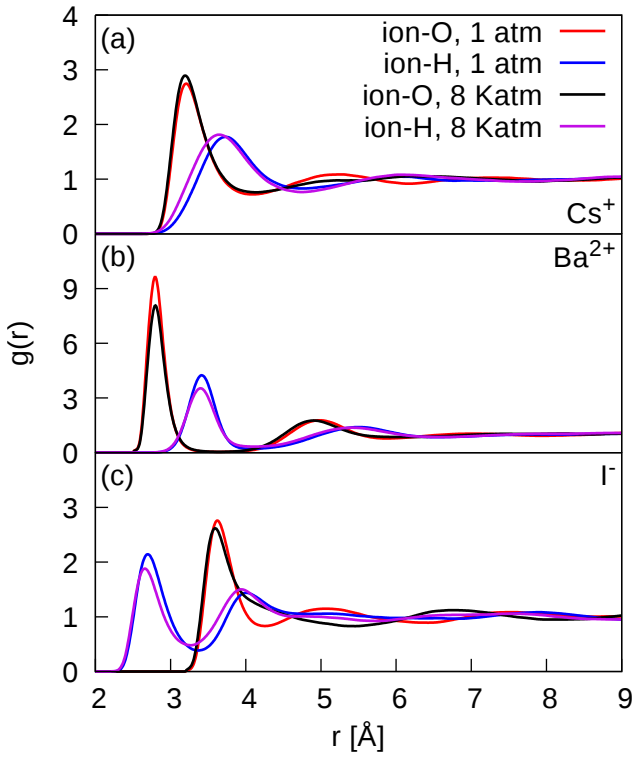

Figure 1: Ion-O and ion-H radial distribution functions for Cs^+ in panel (a), Ba^{2+} in panel (b) and I^- in panel (c) at 298.15 K and pressures of 1 atm and 8000 atm. Results obtained using PBC from NPT MC simulations of a single ion at the centre of a cubic box of 512 TIP4P waters.

and $ion - H$ rdfs shown in Fig. 1. Here we provide only a representative selection of the cases studied in this work, Cs^+ for the alkali metal, Ba^{2+} for the alkaline earth metal and I^- for the halide ions. For each atomic group, these cases correspond to the largest ion within those studied in this work. In the figure, the $ion - O$ and $ion - H$ rdfs are shown at ambient conditions and at 8000 atm and 298.15 K. Details of these rdfs in the whole range of pressure are shown in Fig. 2. For the sake of completeness rdfs for all the

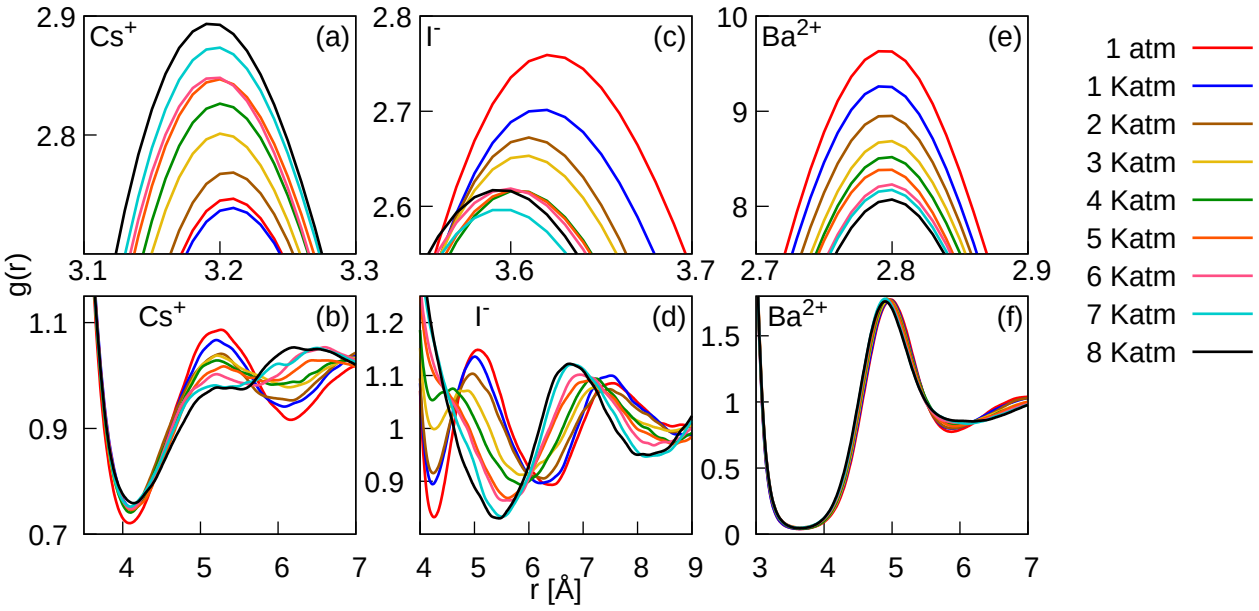

Figure 2: Magnification of the $ion - O$ radial distribution functions around the first maximum position (for Cs^+ (a), for I^- (c), for Ba^{2+} (e)) and from distances around the first minimum to distances around the second minimum (for Cs^+ (b), for I^- (d) and for Ba^{2+} (f)). Results were obtained from MC NPT simulations of a single ion at the centre of a cubic box of 512 TIP4P waters at 298.15 K and pressures from 1 up to 8000 atm.

cases we have studied are provided in the supplementary material (Figs. S1-S16 and Tables S1-S24). In the following two subsections we discuss maxima and minima positions of the rdfs, and how the increasing pressure affects the rdfs' values at the first and second peak.

3.2.1. Changes of rdfs' maxima positions and shell definition upon increasing pressure

An overall look at the rdfs' plots reveals that positions of the maxima and minima are more affected by increasing P the weaker the ion field is. (See Fig. 1, Fig. 2 and Figs. S1-S16.) This is in line with what has been found

Table 4: The first maximum and minimum positions of the ion-O rdf for Cs^+, Ba^{2+}, I^- in TIP4P water at 298.15 K and various pressures from 1 up to 8000 atm. Units of Å[(a)].

	Cs^+		Ba^{2+}		I^-	
P(atm)	r_{max}	r_{min}	r_{max}	r_{min}	r_{max}	r_{min}
1	3.21	4.09	2.79	3.64	3.62	4.26
1000	3.21	4.14	2.79	3.64	3.62	4.23
2000	3.21	4.11	2.80	3.64	3.61	4.24
3000	3.20	4.11	2.80	3.67	3.61	4.26
4000	3.20	4.10	2.80	3.65	3.60	4.23
5000	3.20	4.11	2.80	3.65	3.60	5.61
6000	3.20	4.11	2.80	3.64	3.60	5.54
7000	3.20	4.09	2.80	3.63	3.60	5.51
8000	3.19	4.14	2.80	3.64	3.59	5.46

[a] Statistical uncertaintes of 0.01$\AA$

in other works [10, 11, 13], even if P and T conditions are different from this work.

Shortened distances at the first maximum are clearly shown for Cs^+ among the alkali metal ions and for both halide ions studied, Br^- and I^-. This occurs both for $ion-O$ and $ion-H$ rdfs (Fig. 1 and Figs. S5, S6, S13, S14, S15 and S16). For alkaline earth ions, hydration shells preserve their definition since very small changes are observed only for the position of the first minimum and the second maximum (Table 4 and Tables S10, S13 and S16).

Minima positions are only slightly affected by increasing pressure, except for halide ions, for which the shells' definition drastically changes at pressures higher than 4000 atm. Nevertheless, changes in the $ion-H$ rdfs are significant but regular in these cases (Figs. S13-S16).

In the case of anions' rdfs, more pronounced changes in maxima and minima positions are observed with respect to cations of opposite charge. This is highlighted in Fig. 2, where the effect of increasing pressure on $Cs^{+}-O$ and $I^{-}-O$ rdfs is shown in specific regions, for distances around the first maximum (panels (a) and (c)) and beyond the first hydration shell (panels (b) and (d)). Values of the rdf increase with pressure at the first minimum and decrease at the second maximum in both cases. However, the resulting evolution of the rdfs is quite different. For Cs^{+}, the second peak flattens, hardly affecting the definition of the first shell (panel b). For I^{-}, the second shell collapses into the first shell at pressures higher than 4000 atm (panel d). By contrast, details of the $Ba^{2+}-O$ rdf shown in panels (e) and (f) of the figure illustrate the weakness of the effect of increasing pressure on the shell definition of alkaline earth ions.

Finally, our results on ion hydration under pressure cannot be compared with experimental and simulation results from other studies because these were obtained at temperatures higher than 298 K and very high pressures, generally higher than 10 Katm [10, 11, 13]. However, even in these works it has been found that the hydration shells of Br^{-} and I^{-} are greatly affected by changes of pressure much more than those of cations of a similar size.

3.2.2. Changes upon increasing pressure of the rdf value at maxima positions

As noted above, for the alkaline earth metal ions the position of the first maximum remains practically unvaried under increasing pressure at 298.15 K, but at the same time the greater strength of the ion field determines a larger variation of the value of the rdf at the first maximum position. This can be appreciated in Fig. 3, where the difference between the value of the ion-O rdf at pressure P with respect to 1 atm is plotted versus P. (Data are provided in Tables S1, S4, S7, S10, S13, S16, S19 and S22).

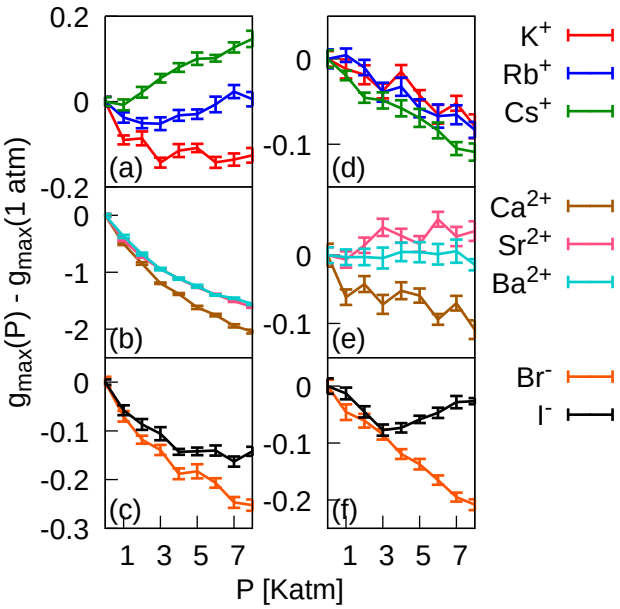

Figure 3: Difference at maxima positions between the ion-O rdf value at a pressure P and that at 1 atm plotted versus pressure for all the ions studied at T=298.15 K and pressures from 1 up to 8000 atm. Results from NPT MC simulations of a single ion at the center of a cubic box of 512 TIP4P waters. Panels (a)-(c) refer to the first peak for alkali metal (a), alkaline earth (b) and halide (c) ion-O rdfs. Panels (d)-(f) refer to the second peak for alkali metal (d), alkaline earth (e) and halide (f) ion-O rdfs.

For Sr^{2+} and Ba^{2+} the curves practically coincide, while for Ca^{2+} the curve decreases with a larger slope from 3000 atm up to 8000 atm (panel (b) of Fig. 3). In the remaining cases, these differences can be roughly tenfold or even smaller. For alkali metal ions the curve of Rb^{+} is in between those of K^{+} and Cs^{+}, for which the slope of the curve becomes positive at a pressure higher than 1000 atm (Fig. 3 (a)). Instead, for both halide ions the curves decrease (Fig. 3 (c)).

We reiterate here that a positive slope of the value of $g(r_{max})$ vs P is typical of hard-sphere cavities in water [9]. For a cavity with a contact radius of 2.85 Å, which is close to the position of the first maximum of the $K^{+}-O$ rdf, at 1000 atm and 8000 atm the rdf value at contact is larger with respect to ambient pressure respectively of 0.37 and 2.06. This effect becomes more important with larger cavities [9]. Thus, trends in Fig. 3 (a)-(c) are generally in agreement with the expectation that curves would deviate more from that relative to a cavity in water of comparable size the stronger the ion field is. In particular, in the case of the alkaline earth ions the effect of increasing pressure is clearly the opposite to that shown in the case of a cavity. Furthermore, with regard to the ion-size effect, since a size increase leads to less negative or even to positive variations (Rb^{+} and Cs^{+}) for a positive variation of P, this appears in line with the behaviour observed for cavities in water [9].

Differently from the first shell peak, as regards the second maximum of the rdf, panels (d)-(f) of the same figure show that in the case of alkaline earth ions there is the smallest effect. For Ba^{2+}, changes produced by increasing pressure are even smaller than statistical uncertainties. For all alkali metal

ions the curves slightly decrease. A greater effect is observed in the case of halide ions, in particular for Br^-, whose curve decreases in the whole range of pressures. For I^- changes are significant with an inversion of trend of around 3000 atm.

More structured hydration shells are commonly revealed in the $ion - O$ rdfs by a sharper peak, to which there would correspond a larger difference of the rdf's values between the maximum and the minimum positions. From our study it emerges that the main effects on $ion - O$ and $ion - H$ rdfs (Figs. S1-S16) determined by increasing P at ambient T are: (1) the decrease of values at the first maximum position, except for Cs^+ and for Rb^+ at pressures higher than 4000 atm (Fig. 3); (2) the slight increase of values at the first minimum position and (3), as a consequence of previous points generally there might be some loss of structure in the first shell. However, at $ion - O$ distances between the first maximum and first minimum, the increase of rdf's values appears to be very important as it implies that the coordination number increases under increasing pressure. These are discussed in Section 3.4, while hydration shell structure results are presented for water dipole orientations in the following section.

3.3. The effect of increasing P on water orientation

3.3.1. Water dipole orientation in the first hydration shell

Tables 5-7 report results averaged on the waters belonging to the first hydration shell, for the angle between the water dipole and the $ion - O$ direction at the various pressures along the isotherm at 298.15 K. This angle is important because the ion-water interaction energy is dominated by the charge-dipole term, which is related to the dot product of the water dipole

moment with the electric field of the ion ($-\mathbf{d} \cdot \mathbf{E}_{ion}$).

Table 5: Pressure dependence at 298.15 K of the average of α^a in the first hydration shell of alkali metal ions in TIP4P water.

	$\langle\alpha\rangle(^\circ)$		
P(atm)	K^+	Rb^+	Cs^+
1	50.3(2)	52.8(1)	56.2(1)
1000	51.2(2)	53.7(2)	57.8(2)
2000	52.2(3)	55.0(2)	58.5(2)
3000	53.0(2)	55.9(2)	59.4(2)
4000	53.5(1)	56.3(2)	59.9(2)
5000	54.2(2)	57.0(2)	60.5(2)
6000	54.7(2)	57.8(2)	60.9(2)
7000	55.4(2)	57.9(2)	60.8(2)
8000	55.9(2)	59.2(1)	62.6(2)

[a] α is the angle between the water-dipole and the ion-O direction.

In *vacuo* the minimal energy configuration corresponds to a value of this angle of 0° in the case of cations and of 180° in the case of anions. Deviations from these values are observed in the liquid phase because of water-water interactions, which are less effective in the case of a stronger ion field. Thus, the magnitude of this angle (α) is more than doubled when comparing results for hydration shells of alkali metal ions (Table 5) with those of alkaline earth ions (Table 6). In the first shell of halide ions, water-water interactions lead to even larger deviations (Table 7). For example, at ambient conditions, in the case of Br^- the value of $\langle\alpha\rangle$ is 125.7°, which corresponds to a deviation

Table 6: Pressure dependence at 298.15 K of the average of α^a in the first hydration shell of alkaline earth ions in TIP4P water.

	$\langle\alpha\rangle(^\circ)$		
P(atm)	Ca^{2+}	Sr^{2+}	Ba^{2+}
1	22.4(1)	25.0(1)	26.8(2)
1000	23.1(1)	25.6(1)	27.7(1)
2000	23.4(1)	26.3(1)	28.7(2)
3000	23.9(1)	26.6(1)	29.2(2)
4000	24.1(1)	27.0(1)	29.7(1)
5000	24.6(1)	27.4(1)	30.1(1)
6000	24.9(1)	27.7(1)	31.0(1)
7000	25.2(1)	28.2(1)	31.2(1)
8000	25.7(1)	28.4(1)	31.5(1)

[a] α is the angle between the water-dipole and the ion-O direction.

of -54.3° from the angle of the most stable orientation *in vacuo*.

Also the ion size affects the ion-field strength felt by the waters, and, as a consequence, the bigger is the ion the larger is the deviation from α_{vacuo} observed at any pressure. As regards the systems studied in this work, this occurs for Cs^+, Ba^{2+} and I^-, respectively for ions of charge +1, +2 and −1 (Tables 5-7).

What is clear from our results is that the higher is the pressure the less favorable is the ion-dipole interaction. Indeed, upon increasing pressure, $\langle\alpha\rangle$ increases in the case of cations and decreases in the case of anions, with larger variations for weaker fields. The difference in $\langle\alpha\rangle$ between 8000 and 1 atm is

Table 7: Pressure dependence at 298.15 K of the average of α^a in the first hydration shell of halide ions in TIP4P water.

	$\langle\alpha\rangle(^\circ)$	
P(atm)	Br^-	I^-
1	125.7(1)	123.9(1)
1000	125.2(1)	123.0(1)
2000	124.7(1)	122.0(1)
3000	124.0(1)	120.4(1)
4000	123.7(2)	119.9(1)
5000	122.8(2)	106.3(1)
6000	121.8(2)	106.2(1)
7000	121.3(2)	106.1(1)
8000	118.0(2)	105.9(1)

[a] α is the angle between the water-dipole and the ion-O direction.

302 5.6° for K^+ and 6.4° for Cs^+. In the case of alkaline earth ions, this difference
303 is smaller, 3.3° for Ca^{2+} and 4.7° for Ba^{2+}. However, variations are larger
304 in the case of halide ions, likely because of the significant variation of the
305 first shell radius discussed in Section 3.2. For Br^- and I^- $\langle\alpha\rangle$ differences are
306 respectively of 8° and 18°.

307 *3.3.2. Water dipole orientation at a given distance from the ion*

308 What has been said above could be misleading as regards the ion-water
309 dipole interaction because it is based on the angle averaged on the shell.
310 Thus we computed also $\langle cos(\alpha)\rangle$ averaged on water molecules whose oxygen

distance from the ion center is r. Fig. 4 shows this quantity for Cs^+, Ba^{2+} and I^- at some pressures along the isotherm at 298.15 K. The small values

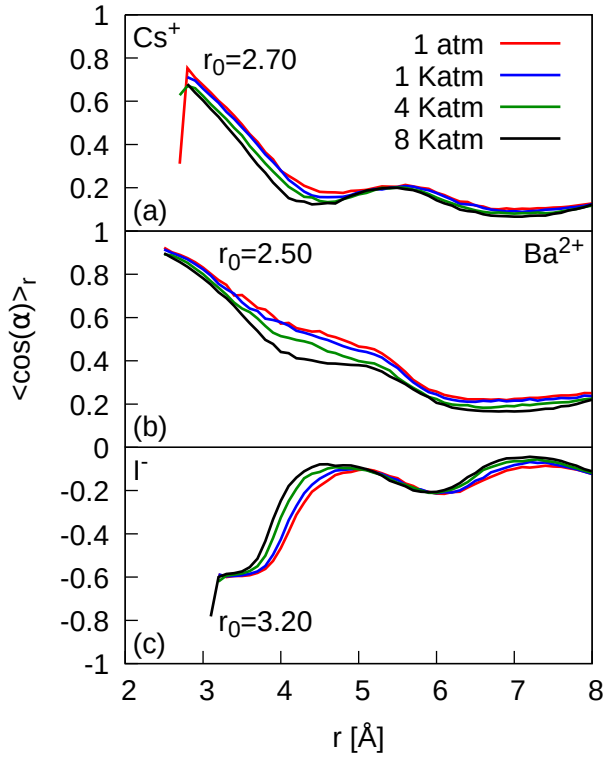

Figure 4: Radial dependence of $\langle cos(\alpha)\rangle_r$ for waters whose oxygens are at distance r from the ion, averaged in the spherical shell of radius r and thickness 0.1 Å, studied as a function of pressure from 1 to 8000 atm at T=298.15 K. Results averaged on 26K configurations saved from the Monte Carlo simulation of a single ion at the centre of a cubic box of 512 water molecules with PBC in a NPT ensemble. Panel (a) contains the results obtained for Cs^+ ion, panel (b) for Ba^{2+} and panel (c) for I^-.

observed for r beyond the second shell indicate that in this region the ion field has lost most of its capability to orient water molecules, particularly in the case of I^-.

However, apart from a very limited range of r, in which the dipole ori-

entation has practically the same average value as at 1 atm, the ion-dipole interaction is almost always destabilized upon increasing pressure. Depending on the ion, this effect is more significant in different regions, involving all distances of the first shell in the case of Cs^+, a wide region between the tail of the first peak and the shoulder of the second peak in the case of Ba^{2+} and the region between the first maximum and the first minimum of rdf in the case of I^- (see Table 4). In these regions, the curves have almost regular shifts towards shorter distances at higher pressures in all cases. This effect is similar to that observed on the ion-H rdfs and very dissimilar to that observed on the ion-O rdfs of Cs^+ and I^- (Fig. 2).

The collapse of the second shell of I^- into the first shell by means of isothermal compression hints that the boundary between the two shells is inadequately defined by the minimum of the I^--O rdf at higher pressures. A more appropriate definition can be based on the point of inflection of the curve of $\langle cos(\alpha)\rangle_r$, whose position changes from 4.12 Å at 1 atm to 3.87 Å at 8000 atm (Fig. 4 (c)). The minimum of the I^--O rdf is located very close to these values at pressures lower than 4000 atm. Furthermore, the position of the second peak of the I^--H rdf is found nearby (within 0.08 Å), regardless of the pressure. This peak receives contributions from both water molecules whose oxygen is in the first shell and molecules whose oxygen is in the second shell. This reinforces the idea that this distance correctly defines the boundary of the first shell of I^-.

On closer analysis, by using the inflection point of $\langle cos(\alpha)\rangle_r$, the first shell is characterised by a greater probability for orientations with negative cosine, while the probability of orientations with positive cosine becomes

comparably significant already at the distance of minimum of the rdf. By adopting this shell definition, compression yields very small changes in $\langle\alpha\rangle$, the difference between 8000 atm and ambient pressure being within $\sim 2^\circ$ for both halide ions. A consistent boundary for the second shell can be fixed by using the inflection point of the curves that is located in the second range where the slope is positive (Fig. 4 (c)). The corresponding ion-O distances slightly decrease with increasing pressure, from 6.55 Å to 6.43 Å in the case of I^- and from 6.26 Å to 6.15 Å in the case of Br^-. Therefore, also for the second shell, values are close to the ambient pressure value of the rdf's second minimum.

3.4. The effect of increasing P on cn

3.4.1. Shells defined by the minima of the ion-O rdf

The values of the ion-O rdfs obtained from the MC simulations were interpolated by a cubic spline, which was examined to determine the position of the first and the second minimum. These were used to define r_1 and r_2 and hence the coordination numbers of the first and second hydration shells were computed from eq. 2 and eq. 3. Panels (a)-(f) of Fig. 5 show the results plotted against the pressure.

As regards the first hydration shell, a significant increase of the coordination number is generally observed as pressure increases (panels (a)-(c) of Fig. 5). For the alkali metal ions, cn_I increases from 7.3 up to 8.7 in the case of K^+ and from 8.7 up to 11.4 in the case of Cs^+. For the alkaline earth ions, the increase is smaller, from 8.8 up to 9 in the case of Sr^{2+} and from 9.2 up

to 9.8, in the case of Ba^{2+}, while for Ca^{2+} variations are almost negligible.

Of the halide ions, the most striking effect is observed on I^- between 4000 and 5000 atm, where the gap in the coordination number is determined by the drastic change in r_{min} (see Tab. 4). Fig. 5 (c) shows also opposite trends of cn_I at lower and higher pressures with respect to the region where the gap occurs. Up to 4000 atm, cn_I increases from 8.4 up to 9.7, while in the range between 5000 and 8000 atm, cn_I decreases from 26.1 to 25. For Br^- the first shell maintains its definition and cn_I increases from 7.8 up to 11.

As regards the second shell, changes of r_2 upon increasing pressure can be more important and as a consequence a change of behaviour is observed at higher pressures, greater than 5000 atm (panels (d)-(f) of Fig.5). These changes are more important for the ions of a larger size: the coordination number shows a striking decrease for Cs^+ and an increase for Ba^{2+}. Because waters are more distant from the ion, the most important changes are shown in the case of I^- with a profile of cn_{II} that reflects the important changes in cn_I. Nevertheless, it can be noted that before the region where the gap occurs, at a pressure less than 3000 atm cn_{II} mainly decreases with values very close to those of the Br^- shell. The decreasing trend of cn_{II} in all the range of pressures seems to be characteristic of Br^-.

3.4.2. An alternative shell definition for halide ions

The above description of the isothermal compression on the coordination number of I^- is within the most common boundary definition. For the first hydration shell, an alternative description is provided by the boundary

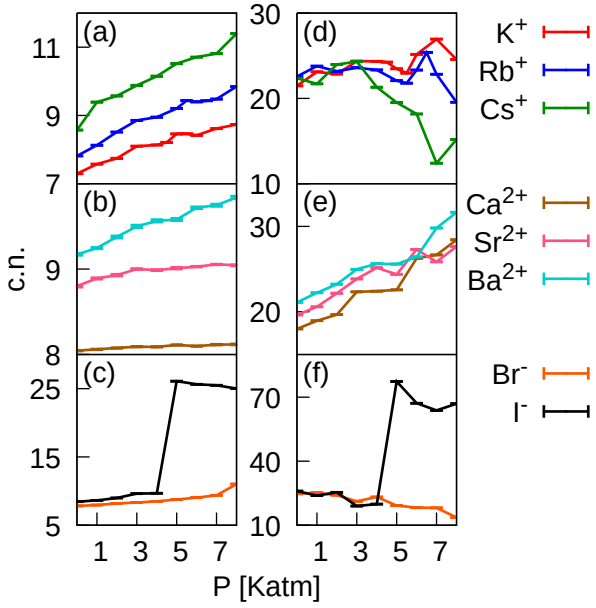

Figure 5: Coordination numbers as a function of pressure for all the ion-water systems studied from 1 up to 8000 atm at T=298.15 K. Results from NPT MC simulations of a single ion at the center of a cubic box of 512 TIP4P waters. Panels (a)-(c) refer to the first shell of alkali metal (a), alkaline earth (b) and halide ions (c). Panels (d)-(f) refer to the second shell of the ions.

defined by the position of the inflection point of $\langle cos(\alpha)\rangle_r$, which has been proposed in section 3.3.2. The increase in pressure results in a slight contraction of this shell, while the coordination number tends to remain almost constant. The coordination number is about 7.4 at almost all pressures, except at 1 atm (7.5), at 7000 atm (7.3) and at 8000 atm (7.1). Therefore, there is a very weak tendency to decrease.

At pressures higher than 4000 atm, the region defined by the two alternative boundaries of the first shell corresponds to the second shell collapsed into the first shell. The average number of oxygens in this region varies from

18.7 at 5000 atm to 18.0 at 8000 atm. These values therefore connect without gap to cn_{II} computed at 4000 atm for r_1 and r_2 fixed at the minima of the rdf. The resultant curve should be very close to that of Br^- (panel (f) of Fig.5). On the contrary, by adopting the alternative definition also for the boundary of the second shell, results show a slight contraction of the shell (fig.4 (c)). Results of cn_{II} increase from $\sim$ 29 at 1 atm up to 34.6 at 8000 atm, with a value of $\sim$ 31.7 at the plateau between 4000 and 6000 atm. As well as for I^-, the alternative boundary definition of the first shell yields for Br^- a cn_I almost constant along the isotherm (7.4-7.5). The pressure profile of cn_{II} is non-monotonic with changes from $\sim$ 21 at 1 atm up to 29.5 at 8000 atm.

3.5. Hydration shell contribution to the excess volume of ions

Figure 6 shows how ΔV_{shell_I} is affected by the increase in pressure at isothermal conditions (298.15 K). In all the cases, the first shell contribution to the excess volume of ions in very diluted aqueous solutions is negative at all pressures. This means that the first shell is subjected to electrostriction. First, in section 3.5.1 , we discuss the results of ΔV_{shell_I} and its component terms (eq. 8) at ambient conditions by making comparisons between ions (Table 8). Second, in sections 3.5.2 and 3.5.3, we discuss the effect of increasing P on the first and the second shell excess volume contributions, giving an interpretation of the trends shown in Fig. 6 and Fig. 7. Hence, in section 3.6, we discuss the excess electrostrictive volume per water molecule. Finally, in section 3.7, we compare results obtained by using alternative boundaries for the shells of halide ions.

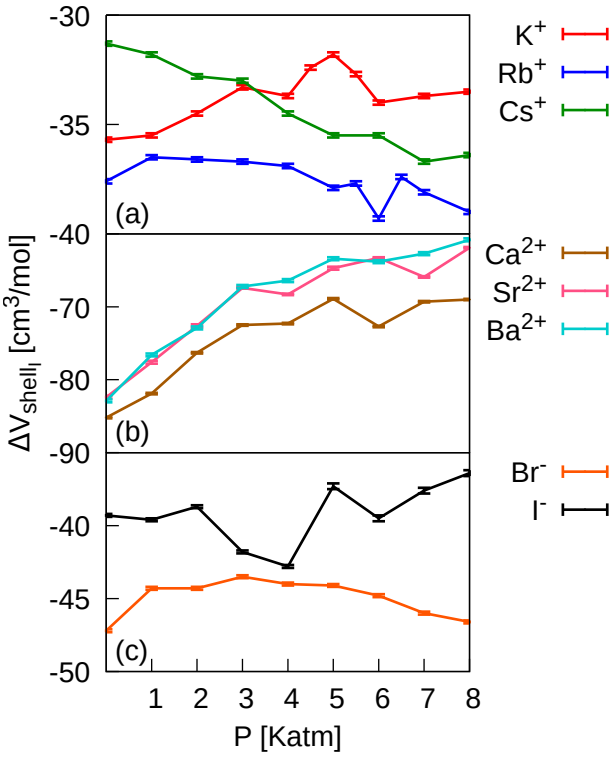

Figure 6: The first hydration shell contribution to the excess volume for the ions in TIP4P water at 298.15 K plotted versus pressure in the range from 1 atm up to 8000 atm. Results obtained from Eq. 8, for alkali metal ions (panel (a)), for alkaline earth ions (panel (b)) and for halide ions (panel (c)). Error bars from error propagation using the standard error on *cn* computed at fixed spherical shell volume defined by r_1 and r_2

3.5.1. The first hydration shell of ions: ΔV_{shell} at ambient conditions

As general behaviour, a more negative ΔV_{shell_I} can be expected when water molecules are subjected to a stronger ion-field. Indeed, for alkali metal ions values are more than halved with respect to those of alkaline earth ions (Table 8) at ambient conditions.

From eq. 8, the negative value is determined by the dominance of the

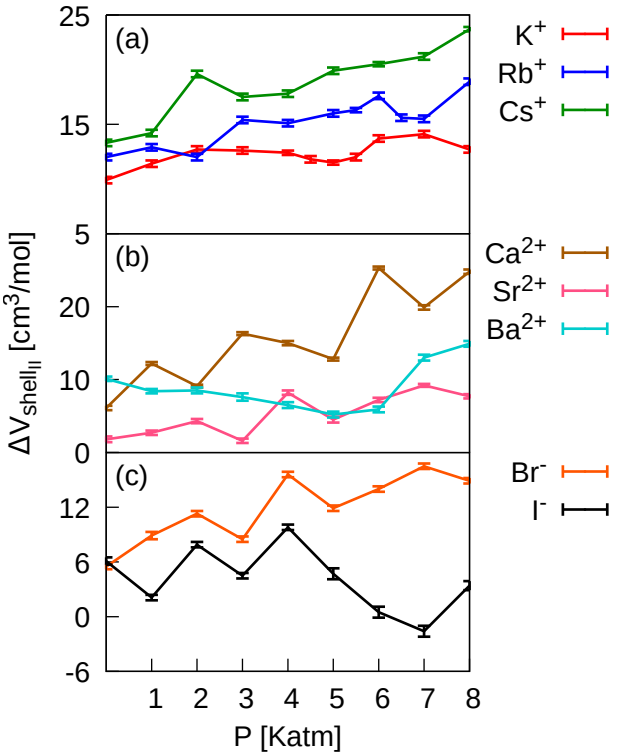

Figure 7: The second hydration shell contribution to the excess volume for the ions in TIP4P water at 298.15 K plotted versus pressure in the range from 1 atm up to 8000 atm. Results obtained from Eq. 9, for alkali metal ions (panel (a)), for alkaline earth ions (panel (b)) and for halide ions (panel (c)). Error bars from error propagation using the standard error on cn computed at fixed spherical shell volume defined by r_1 and r_2

Table 8: Results of ΔV_{shell} for the first hydration shell of the ions at 298.15 K and 1 atm (third column) and the maximum variation under increasing pressure (last column). In the first column the spherical shell volume defined by r_0 and r_1 (second term of eq.8) and in the second column $-cn/\rho_0$ (the first term of eq.8). All the data in cm^3/mol.

		First shell		P
	V_1-V_0	$-cn/\rho_0$	ΔV_{shell}	$effect$
K^+	96.0	-131.7	-35.7	3.9 [c]
Rb^+	103.5	-141.1	-37.6	-1.7 [d]
Cs^+	123.5	-154.8	-31.3	-5.4 [e]
Ca^{2+}	60.1	-145.3	-85.2	16.3 [c]
Sr^{2+}	76.5	-158.9	-82.4	20.5 [f]
Ba^{2+}	82.7	-165.6	-82.9	22.1 [f]
Br^-	94.0	-141.2	-47.2	3.7 [a]
I^-	113.1	-152.5	-39.3	-3.4 [b]

[a] at 3000 atm

[b] at 4000 atm

[c] at 5000 atm

[d] at 6000 atm

[e] at 7000 atm

[f] at 8000 atm

term proportional to the coordination number with respect to the spherical shell volume, although both terms are important in comparison between ions. For example, coordination numbers of Ca^{2+} and Rb^+ are very close (Table 2) and the large difference in ΔV_{shell_I} stems from the smaller spherical shell volume around Ca^{2+} (Table 8). The importance of this term justifies also

the less negative values obtained for the shells of Sr^{2+} and Ba^{2+}, which are larger in size and have larger coordination numbers with respect to Ca^{2+} (Table 2). Nevertheless, differences are within the thermal volume at ambient temperature (2.3 cm^3/mol).

The comparison between alkali metal ions shows small differences within 5 cm^3/mol. In this case, the slightly larger coordination number of Rb^+ with respect to K^+ seems to justify the slightly more negative value of ΔV_{shell_I} of Rb^+. On the contrary, despite the larger difference in coordination number, the opposite occurs in the comparison between Cs^+ and K^+, whose smaller spherical shell volume turns out to be decisive.

Again, in the comparison with the halide ions, the smaller spherical shell volume of the alkaline earth ions is responsible for the large difference observed in ΔV_{shell_I}.

For halide ions, the first shell contribution to the excess volume is more negative than for the alkali metal ions. This is opposite to what is expected from considerations based on the strength of the ion-field felt by waters in the shell. Nevertheless, a clear explanation is provided by the two terms in eq. 8. Indeed, Br^- and Rb^+ have the same coordination number at ambient pressure (Table 2), but the spherical shell volume of Br^- is smaller (Table 8), despite waters in its hydration shell being less close to the center of the ion. This arises from their different orientation in the shell of anions that leads to a larger V_0 (see eq. 8). The same holds for the comparison between I^- and Cs^+, for which coordination numbers are very close at ambient pressure (Table 2). We remind the reader that the shell excess volume was obtained from a definite integral involving the ion-O rdf (eq. 5). The larger distance

of closest approach to the central ion for oxygens in the shell of I^-, which is visible in Fig. 1, determines the significant difference in V_0 with respect to Cs^+.

Finally, by comparing the results of the two halide ions, these are in line with the ion-field strength, but still the more negative shell contribution to the excess volume obtained for Br^- stems from its smaller spherical shell volume with respect to I^- (Table 8).

3.5.2. The effect of increasing P on the first shell contribution to the excess volume

As pressure increases, generally ΔV_{shell_I} becomes less negative for alkaline earth ions and K^+ (Fig.6). Results exhibit the opposite for Cs^+ in the whole range of pressure and for I^- between 2000 atm and 4000 atm. For Rb^+ and Br^-, the quantity tends to become less negative at low pressures while shows the opposite at higher pressures with small variations.

The greatest effect of increasing pressure is observed for the hydration shell of alkaline earth ions with monotonically increasing trends up to 3000 atm. At higher pressures, ΔV_{shell_I} continues to increase but less rapidly and the interpolation of points seems to suggest the presence of some critical point. It is out of the scope of this work to investigate their existence. Here we simply limit ourselves to qualitatively examine these trends.

From eq. 8, the partial derivative of ΔV_{shell_I} with respect to P at constant T has three contributions,

$$\left(\frac{\partial \Delta V_{shell_I}}{\partial P}\right)_T = -\frac{1}{\rho_0}\left(\frac{\partial cn_I}{\partial P}\right)_T + \frac{cn_I}{\rho_0^2}\left(\frac{\partial \rho_0}{\partial P}\right)_T + \left(\frac{\partial (V_1 - V_0)}{\partial P}\right)_T . \quad (10)$$

On the basis of the above equation, a positive slope of a curve in Fig. 6 can reflect the increase in water density upon increasing pressure if the variations of cn_I and the spherical shell volume, $V_1 - V_0$, are less important. This happens for the alkaline earth ions, particularly at pressures less than 4000 atm. At higher pressures, for Ca^{2+} and Sr^{2+} , the non-monotonicity of the curves follows from the slope of the spherical shell volume, despite for the alkaline earth ions the definition of the first shell is quite well maintained upon increasing pressure (Tables 4, S11 and S13). This is not surprising since a change in r_1 of 0.01 Å can produce a change in the spherical shell volume of around 1 cm^3/mol.

The considerations above regarding non-monotonicity are generally valid. However, for alkali and halide ions the coordination number significantly rises at higher pressures (Fig. 5 (a) and (c)) and $-cn_I/\rho_0$ is not monotonic. Moreover, upon increasing the pressure, the variation of this term of eq. 8 is partially balanced by the variation of the spherical shell volume. This explains why the variation in ΔV_{shell_I} along the isotherm is within few cm^3/mol.

Generally, the variation of ΔV_{shell_I} at a pressure P with respect to 1 atm is positive, with some exceptions as in particular for Cs^+ (see Fig.6 and the last column of Table 8). At the same time, differently from the other cases, for Cs^+, $V_1 - V_0$ at 1 atm is always less than at higher pressures. At 1000 and 8000 atm the shell expansion is of 6 cm^3/mol while at pressures in between this remains within 1-2 cm^3/mol. These variations reflect the variations in

r_{min} (Table 4) and lead to a larger increase of the coordination number upon increasing pressure (Fig. 5(a)). The consequent increased importance of the term $-cn_I/\rho_0$ in eq. 8 is at the basis of the observed decrease of ΔV_{shell_I} along the isotherm (Fig. 6(a)).

The three curves in Fig. 6(a) show very different profiles. This underlines how shells progressively more affected by the increase in pressure determine a different pressure dependence of ΔV_{shell_I}, passing from K^+ to Rb^+ and from Rb^+ to Cs^+. For K^+ the curve is qualitatively similar to that of Ca^{2+} (Fig. 6(b)). Its monotonic increase up to 3000 atm still indicates the dominance of the second term in eq. 10, which for K^+ is less positive than for Ca^{2+}, as a consequence of a smaller cn_I (see Fig.5 and Tables S2 and S11). Also the behaviour at higher pressures is clearly non-monotonic with a local maximum of around 5000 atm.

Of the halide ions, Br^- presents a pressure profile of ΔV_{shell_I} similar to that of Rb^+. The two curves share a small increase at 1000 atm with respect to 1 atm and a large interval of pressures, up to 4000 atm in the case of Rb^+ and up to 5000 atm in the case of Br^-, in which ΔV_{shell_I} is very little affected by the increase in pressure. At a higher pressure, the two curves differ in some details (a local minimum is present in the case of Rb^+) but from 6000 up to 8000 atm both show again a similar behaviour with a negative slope. This similarity arises from the combination of the three terms in eq. 10, as, upon increasing pressure, cn_I of Br^- increases with a larger slope and the spherical shell volumes of the two ions show dissimilar behaviours.

However, ΔV_{shell_I} shows a very particular pressure profile for I^-, owing to its shell being very strongly affected by the increase in pressure. As remarked

in previous sections, the most important effect is the gap in cn_I between 4000 and 5000 atm (Fig.5 (c)), which is determined by a shift of 0.4 Å in the first minimum position of the $I^- - O$ rdf (Table 4). At 5000 atm, ΔV_{shell_I} is less negative than at 4000 atm of 5.5 cm^3/mol. This variation is therefore dominated by the increase of the spherical shell volume (eq. 8). On the contrary, the monotonic increase of cn_I at lower pressures, between 2000 and 4000 atm, is determinant for the negative slope of the pressure profile in Fig. 6 (c). At higher pressures, between 6000 and 8000 atm, cn_I increases quite slowly while there is a clear contraction of the spherical shell volume (Table S22). Both cannot explain the positive slope of the curve, for which the increase of water density (second term of eq. 10) seems to be determinant.

3.5.3. The effect of increasing P on the second shell contribution to to the excess volume

Differently from the first shell, as shown in Fig.7, the second shell's contribution to the excess volume of the ions' aqueous solutions is positive in all cases but one (I^- at 7000 atm). This implies that the spherical shell volume is generally the dominant term in eq. 9, although the negative term is affected by increasing pressure because of the very important changes of the second shell coordination number (panels (d)-(f) of Fig. 5). For these reasons, the analysis of the effect of increasing pressure on $\Delta V_{shell_{II}}$ can appear more complicated than for the first shell's contribution. Nevertheless, results can be interpreted on the basis of an analogous equation to Eq. 10 derived for the second shell from Eq. 9,

$$\left(\frac{\partial \Delta V_{shell_{II}}}{\partial P}\right)_T = -\frac{1}{\rho_0}\left(\frac{\partial cn_{II}}{\partial P}\right)_T + \frac{cn_{II}}{\rho_0^2}\left(\frac{\partial \rho_0}{\partial P}\right)_T + \left(\frac{\partial (V_2 - V_1)}{\partial P}\right)_T . \quad (11)$$

For instance, the first term of the equation above can contribute to a positive slope at a higher pressure for alkali metal ions (see Fig. 7(a)) because cn_{II} decreases with P (see Fig.5(d)). For Cs^+, this occurs in a wide range, from 3000 atm up to 7000 atm, where the third term gives a negative contribution. For alkaline earth ions, generally cn_{II} increases (see Fig.5(e)), giving a negative contribution to the slope of $\Delta V_{shell_{II}}$. However, for the curve of Ca^{2+} (fig. 7(b)), from 3000 atm up to 6000 atm, the negative slope appears to be mainly determined by the contraction of the spherical shell volume (third therm of Eq. 11) as variations of the coordination number are very small in this range. To give another clear example, for I^- (Fig. 6(f)), the slope is negative from 4000 atm up to 7000 atm, but in this range, apart from the gap, cn_{II} decreases, so that the contraction of the spherical shell volume is more important.

Finally, the first shell's contribution to the excess volume is always much more important than the second shell contribution, especially for the alkaline earth ions. Thus the sum of the two contributions is negative. It is worth commenting on changes under pressure of the relative importance of the two contributions. For all cases considered in Table 9, with the exception of I^-, the ratio $-\Delta V_{shell_{II}}/\Delta V_{shell_I}$ significantly increases at higher pressures. An inspection of the data (Tables S1-S24) shows that this correspondingly implies less negative ΔV_{shell_I} and more positive $\Delta V_{shell_{II}}$. For the specific cases of I^-, in which the opposite occurs, as for instance comparing 1000

Table 9: Results for the ratio of ΔV_{shell} between the second and the first hydration shell of the ions studied in this work at T=298.15 K and at some pressures along the isotherm.

	P			
	1 atm	1 $katm$	4 $katm$	8 $katm$
K^+	-0.279	-0.322	-0.367	-0.379
Rb^+	-0.320	-0.352	-0.409	-0.485
Cs^+	-0.423	-0.447	-0.515	-0.652
Ca^{2+}	-0.072	-0.149	-0.207	-0.360
Sr^{2+}	-0.021	-0.035	-0.121	-0.124
Ba^{2+}	-0.122	-0.110	-0.098	-0.245
Br^-	-0.116	-0.202	-0.354	-0.319
I^-	-0.155	-0.052	-0.229	-0.092

atm with 1 atm, or 8000 atm with 4000 atm, both seem characterised by a less positive $\Delta V_{shell_{II}}$ at the higher pressure. The ratio shows also dependence on the specific ion. For alkali metal ions, at any pressure, the ratio increases with the ion size. The same occurs only when comparing Ba^{2+} with Sr^{2+} and Ca^{2+}. The relative importance of ΔV_{shell_I} and $\Delta V_{shell_{II}}$, strikingly depends on the ion and on the pressure (Table 9). This has relevance regarding the evaluation of the excess volume from KB integrals (Eq. 4), as it could imply that correspondingly a different cutoff would be required in order to obtain

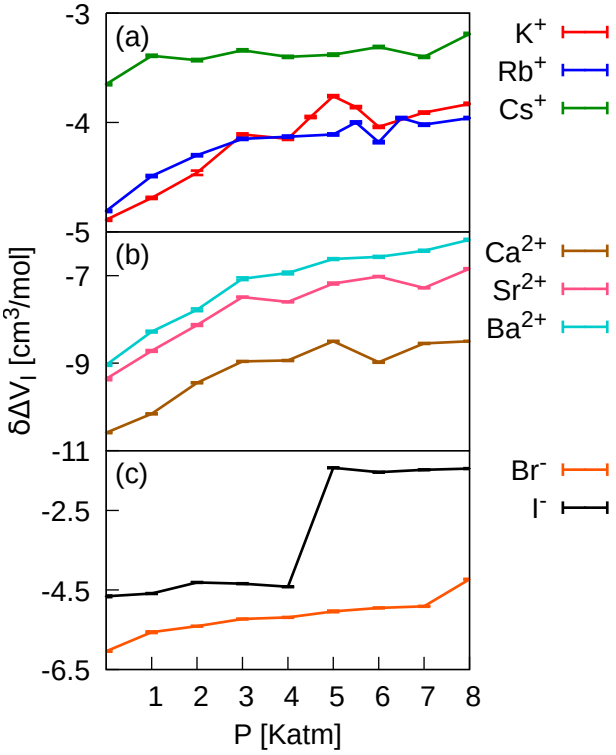

Figure 8: The first hydration shell contribution to the excess volume normalized to cn_I for the ions in TIP4P water at 298.15 K plotted versus pressure in the range from 1 atm up to 8000 atm. Results for alkali metal ions in panel (a), for alkaline earth ions in panel (b) and for halide ions in panel (c).

a given accuracy.

3.6. The effect of increasing P on the shell electrostrictive volume per molecule

In the literature, the excess volume of ions in an aqueous solution has been used to determine electrostriction [26, 2]. Our simulation results show that electrostriction is not homogenous, and strictly regards the first hydration shell of the ions (Fig. 6), as the second shell is subjected to a volume expansion with respect to pure solvent (Fig. 7).

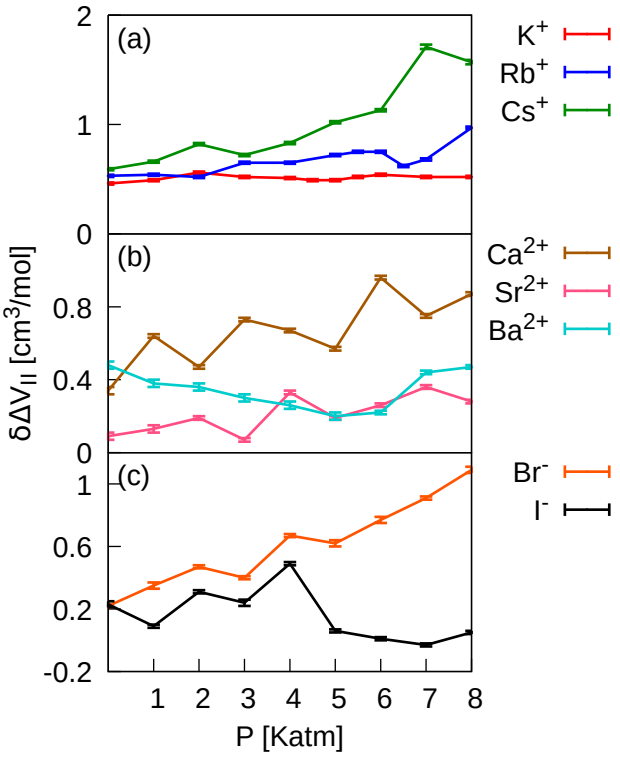

Figure 9: The second hydration shell contribution to the excess volume normalized to cn_{II} for the ions in TIP4P water at 298.15 K plotted versus pressure in the range from 1 atm up to 8000 atm. Results for alkali metal ions in panel (a), for alkaline earth ions in panel (b) and for halide ions in panel (c).

The shell excess volume normalized to the corresponding coordination number equals the difference between the inverse of the local number density averaged on the shell and the inverse of the number density in pure water. As regards the first shell of an ion, by reversing the sign of this quantity we obtain the shell electrostrictive volume per molecule, which allows us to make a more consistent comparison between ions and gives a new insight into the pressure effect.

At any pressure along the isotherm, the first shell's electrostrictive volume per molecule (Fig. 8) is larger for alkaline earth ions with the order expected on the basis of the field strength, $Ca^{2+} \succ Sr^{2+} \succ Ba^{2+}$. However, values relative to the hydration shell of Sr^{2+} and Ba^{2+} are very close. For Ba^{2+}, at 8000 atm, the shell's electrostrictive volume per molecule is smaller than that at 1 atm of 2.8 cm^3/mol. This is the largest decrease in the quantity we observed along the isotherm upon increasing pressure.

For the alkali metal ions the sequence $K^+ \succ Rb^+ \succ Cs^+$ is generally respected. The shell electrostrictive volume per molecule in the shells of K^+ and Rb^+ show very close values, in particular between 2000 and 3000 atm and the order above is inverted in the range 4000-6000 atm (Fig. 8 (a)). On the contrary, at any pressure, the curve relative to the first shell of Cs^+ is well separated from the curves of the other two alkali metal ions. In this case, it is interesting that the shell electrostrictive volume per molecule remains unaffected by the increase of pressure in a very large range, between 1000 and 7000 atm. The most relevant effect in this range is the increase in the coordination number, the spherical shell volume being little affected, as noted at the end of Section 3.5.2. The behaviour above means that the local number density of oxygens in the shell increases upon increasing pressure with a slope which is close to that of the number density of TIP4P water.

For halide ions, at any pressure along the isotherm, the shell electrostrictive volume per molecule increases with the expected order: $Br^- \succ I^-$. However, when comparing the shell of Br^- with the shell of alkali metal ions, the order of increase of the same quantity, $Br^- \succ K^+$, is unexpected on the basis of the ion-O distances. The same considerations made in the

previous sections when comparing ΔV_{shell_I} can be repeated here. The interplay between ion-water and water-water interactions in the shell of Br^- might be very important in determining larger values. However, differences with respect to the alkali metal ions (Fig. 8 (a)) are reduced at higher pressures, since the quantity is more affected by the increase of the pressure for the shell of Br^- (Fig. 8 (c)).

In the case of I^-, the pressure profile shown in Fig. 8 clearly reflects the underlying structural changes of the shell. At pressures less than 4000 atm, the shell electrostrictive volume per molecule of I^- is larger than that of Cs^+ and is very similar to that of K^+ and Rb^+. At 4000 atm the important change in the definition of the first shell of I^- results in a very low electrostrictive volume per molecule, which is less even than that of Cs^+.

At this point, it is important to remark that also the shell excess volume relative to the first hydration shell of a hydrophobic solute can be negative [15, 9] , but in this case the quantity is not obviously related to electrostriction. For example, for cavities, whose contact radii with oxygen of water is 2.8 Å and 3.3 Å, ΔV_{shell_I} normalized to the coordination number is respectively -2.4 cm^3/mol and -0.5 cm^3/mol, at ambient conditions. At 8000 atm, the same quantity becomes -3.1 and -0.4 cm^3/mol. These cavities seem to be appropriate for comparison with Rb^+ and I^-, as their contact radii fall between r_0 and r_1 of these ions. Thus, the volume contraction per water molecule in the first hydration shell of a monoatomic ion is effectively larger than that in the hydration shell of a cavity of comparable size.

On the contrary, for waters in the second hydration shell there is in the majority of the cases a very slight expansion (Fig. 9) with the general ten-

dency for $\delta\Delta V_{II}$ to increase with increasing pressure. This behaviour is more evident for Br^- and Cs^+, for which the decrease with P in the coordination number (Fig. 5 (d) and (f)) is relevant. With regard to I^-, as well as for the first shell, also the quantity relative to the second shell shows a specific pressure profile. At 4000 atm there is a change of behaviour that causes a very slight contraction of volume per molecule at higher pressures. It is worth noting that, in the same range, $\Delta V_{shell_{II}}$ (Fig. 7) and cn_{II} (Fig. 5 (f)) are both significantly affected by the increase in pressure, while their ratio remains almost constant (Fig. 9).

3.7. How shell volumetric results depend on shell definition

The shell excess volumetric quantities discussed in the previous sections refer to the most common definition of shell. This is based on the minima of the rdf, namely the ion-O rdf in this work. Nevertheless, this definition could be inconvenient when comparing results at different pressures. This happens for I^-, for which we have proposed an alternative boundary definition for the first shell based on the radial distribution of water dipole orientations (section 3.3.2). Here we discuss the corresponding results of ΔV_{shell_I} and the quantity normalised to cn_I for both halide anions. Results are plotted in Fig. 10, in panels (c) and (d) for I^- and in panels (e) and (h) for Br^-.

We have shown before how the two terms of eq. 8 can be both involved in changes caused by compression. In order to esemplify this effect here we introduce two additional shell definitions. One is the shell defined by the first minimum of the rdf at 1 atm. For this shell cn_I increases with pressure, as shown in panel (a) for I^- and in panel (e) for Br^- (blue lines). The

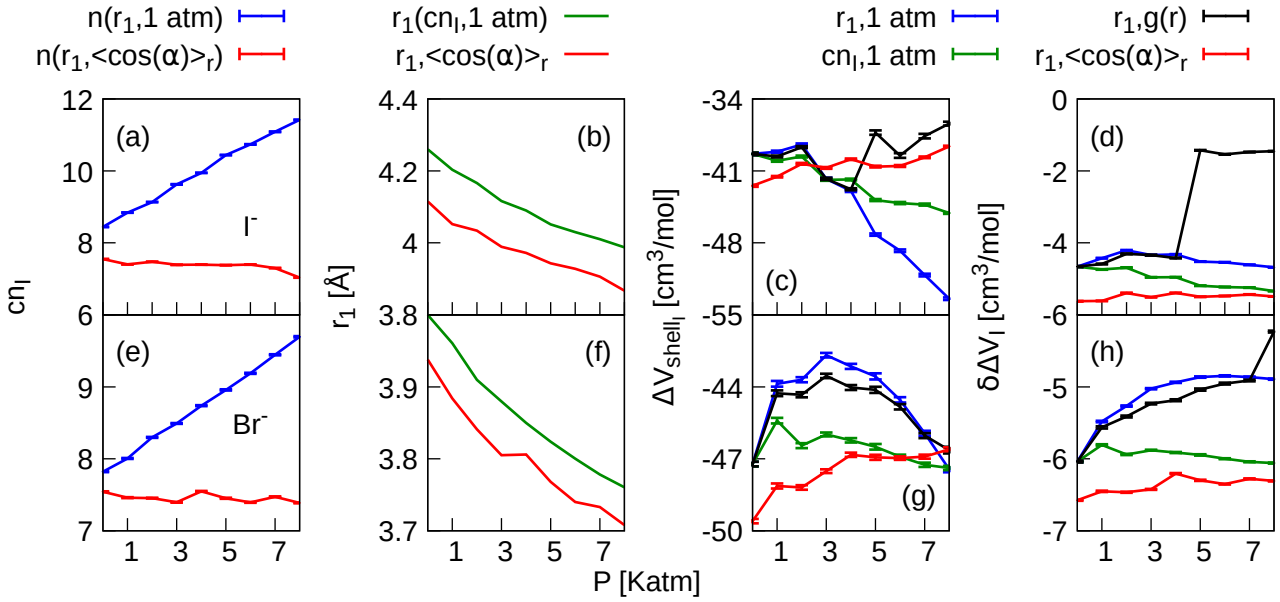

Figure 10: The effect of the boundary shell on pressure profiles of shell quantities for I^- (panels (a)-(d) and for Br^- (panels (e)-(h)). Red curves refer to the boundary (r_1) fixed at the point of inflection of $\langle cos(\alpha)\rangle_r$ (section 3.3.2). Black curves refer to the boundary fixed at the first minimum of the ion-O rdf. Blue curves refer to the boundary fixed at the ambient pressure value of the rdf's first minimum. Green curves refer to the boundary defined by a constant value of cn_I, which correspond to its value at 1 atm when r_1 is fixed at the first minimum of the rdf. The resultant pressure profiles are plotted for cn_I (panels (a) and (e)), for r_1 (panels (b) and (f)), for ΔV_I (panels (d) and (h). (panels (c) and (g)) and $\delta\Delta V_I$ (panels (d) and (h). Results obtained for the ions in TIP4P water at 298.15 K.

other one is the shell defined by a constant cn_I, here fixed to its value at 1 atm determined at the minimum of the rdf. The boundary of this shell contracts for both ions as shown by the green lines in panels (b) and (d). The alternative shell definition based on the inflection point of $\langle cos(\alpha)\rangle_r$ presents some parallels with both. In fact, cn_I is generally constant along the isotherm (panels (a) and (c)), while the boundary contracts (red lines in panels (b)

and (f)).

According to the features above, we expect contributions to the slope of ΔV_{shell_I} which are positive from the increase of ρ_0 and negative from the decrease of $V_1 - V_0$ (see eq. 10). The first affects the pressure profile at lower pressures, within 1000 atm and 2000 atm, respectively for Br^- and I^- (panels (g) and (d)). Its effect tends to become less important at very high pressure, due to the lower compressibility of water. Thus, ΔV_{shell_I} should tend to remain almost constant or to slightly decrease, which appears as the signature of the slight contraction of $V_1 - V_0$. This generally occurs in the range 2000-6000 atm for I^-. The slight increase between 3000 and 4000 atm can still be justified by the increase in ρ_0. At pressures higher than 6000 atm there is a slight increase. This results from the increase in ρ_0 and by a slight decrease in cn_I. Apart from this last detail, for Br^- the curve is similar, even though values are more negative as a consequence of the smaller spherical shell volume (Eq. 8). In fact, with the alternative shell definition, values of cn_I are very close for the two anions (panels (a) and (e)).

The pressure profile of the results obtained by using the additional shell definitions can be interpreted even more clearly. When the value of cn_I is fixed, the negative slope stems from the shell contraction. Its effect can be seen even at 1000 atm and is generally dominant. Differences between the two ions depend on the different value of cn_I, which is larger in the case of I^- of about 0.6. For both ions, this shell definition yields results which are closer to those obtained with the alternative shell definition. Vice versa, when $V_1 - V_0$ is fixed at its value at 1 atm we observe a significant decrease in ΔV_{shell_I} due to a significant increase in cn_I. This is particularly evident

at pressures higher than 2000 atm in the case of I^- and higher than 3000 atm for Br^-. The curve is very close and similar to that obtained with the standard shell definition in the case of Br^-. For I^- this occurs at pressures within 4000 atm, while at higher pressure the two curves follow very different behaviours.

A clearer view is provided by ΔV_{shell_I} normalised to cn_I. Results are in line with the different shell boundaries. Panels (d) and (h) of Fig. 10 show that the most negative values are obtained when the boundary is based on the inflection point of $\langle cos(\alpha)\rangle_r$, regardless of the pressure. The effect of an increase in pressure on this value is very poor (within 0.25 cm^3/mol). Therefore, differently to what is observed with the standard definition of the first shell, even at high pressures I^- presents a larger electrostrictive volume per water molecule than the alkali metal ions. Results obtained with a fixed value of cn_I are less negative with the maximum difference at 1 atm, for both ions. Results relative to the most common shell definition are even less negative. However, the alternative definition maintains the same order of electrostrictive volume between the two halide ions.

For r_1 and r_2 fixed at the inflection points of the curves plotted in Fig. 4, results obtained for the second shell confirm its positive contribution to the excess volume. For the two ions, values practically coincide at 1 atm, while a different compression effect is evident (Fig. 11). Hence, there are similarities with results obtained with the most common shell definition (Fig. 7), albeit when using the alternative shell definition values are more positive of ~ 3

cm^3/mol.

4. Conclusions

On the basis of our results, the effect of an isothermal increase in pressure on the ion-water rdfs at ambient temperature exhibits mainly two aspects: (1) shifts in the peak and minima positions, and (2) changes in the height of the first peak. The former is particularly evident in the case of I^-, which is a typical "structure breaking" ion, while the latter is important for alkaline earth ions, which are considered as "structure making".

Also the ion-water dipole orientation in the first shell is significantly affected, showing a less attractive ion-dipole interaction at higher pressures, with the greatest effect on halide ions. Regardless of the pressure, the same order of the ions has been found by using the mean absolute deviation of $\langle\alpha\rangle_I$ from the value of the angle α corresponding to the most favoured ion-dipole orientation in *vacuo* (see the first column of Table 10). Even though this quantity refers to the first hydration shell, the ions we have studied are ordered according to the Marcus series, which was based on the hydrogen bonding structure of water. Our results suggest that there is some correlation between ion-water orientations in the first shell and water-water orientations beyond the first hydration shells. Furthermore, the extent of the ion-field influence on the ion-water dipole orientation maintains the same order between the ions, at any pressure, as revealed by the radial profile of the cosine of the angle averaged at a given distance from the ion (Fig. 4). The increase in the coordination number of the first shell under increasing pressure follows the same order, with a larger variation for the halide ions.

As remarked in previous sections, in this work, the computed electrostric-

tive volume (ESV) refers to the first hydration shell, as for the second shell we found a positive contribution to the excess volume. "Structure making" ions have the strongest electrostrictive power, as indicated in Table 10. We note that within the "structure breaking" ions the order based on ESV is partially reversed with respect to the Marcus series, as the first hydration shell of halide ions shows a larger electrostrictive volume than that of alkali metal ions. When examining ESV/cn_I, values decrease at higher pressures, thus confirming that the external pressure opposes the ion-field influence on the first hydration shell. The most important effect is on I^- and on the alkaline earth ions, with order related to the ion size (last column of Table 10).

In addition, electrostrictive volumes computed in this work are not directly comparable with those determined from molar volumes of electrolytes in water. When extracted from experimental data, the electrostrictive volume can depend on the counterion and includes contributions to the excess volume beyond the first hydration shell that can be positive, as found for the second shell in this work. However, regardless of the counterion, from experimental data [3], it has been found that I^- has a lower electrostrictive power with respect to Br^-, which is in agreement with our order based on ESV. On the contrary, on the basis of our results on the electrostrictive volume per water-oxygen in the shell (ESV/cn_I), for alkali metal ions we found the same order derived from the experimental data obtained for electrolytes in which the counterion is Cl^- or Br^-.

Finally, shell quantities depend on shell definition and, therefore, the conclusions above are valid for shell boundaries defined by the minima of the $ion - O$ rdf. The boundary defined by the inflection point of the radial

777 distribution of $\langle cos(\alpha)\rangle_r$ is one of the alternative proposed in this work.
778 According to this shell definition, isothermal compression causes only very
779 small changes in cn_I of I^- and Br^-. Also $\langle\alpha\rangle$ and (ESV/cn_I) are less affected
780 when the alternative shell definition is adopted. However, regarding ESV and
781 (ESV/cn_I), the relative order between the two halide ions is maintained.
782 Furthermore, the two further alternative boundary definitions here proposed
783 in the section 3.7 allow a less difficult interpretation of the pressure profiles
784 of shell contributions to the excess volume in terms of eq. 8.

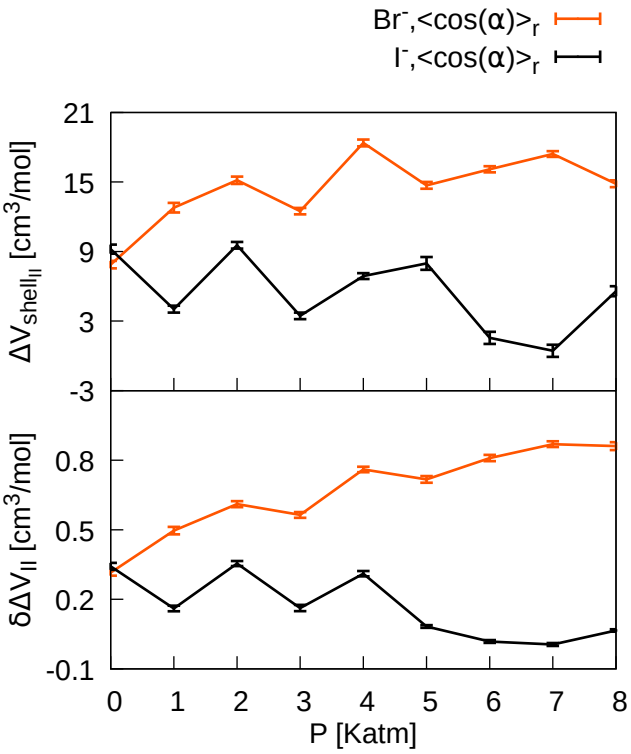

Figure 11: Second shell volumetric quantities obtained for r_1 and r_2 fixed at the points of inflection of $\langle cos(\alpha)\rangle_r$ (section 3.3.2). The resultant pressure profiles of ΔV_{II} (top panel) and $\delta\Delta V_{II}$ (bottom panel) are plotted for I^- (black curve) and Br^- (orange curve). Results obtained in TIP4P water at 298.15 K.

Table 10: Lists of ions based on results of this work (T= 298.15 K) for the quantities: $|\langle\alpha\rangle_I - \alpha_{vacuo}|$ (see section 3.3.1), the electrostrictive volume of the first hydration shell, $ESV = -\Delta V_{shell_I}$ (see section 3.5.1), the electrostrictive volume per water molecule in the first shell, ESV/cn_I , and its variation between 8000 and 1 atm. In each column, ions are ordered from the smallest (top) to the largest (bottom) value of the quantity.

ions' order			
$\Delta < \alpha >_I$ [a]	ESV [b]	ESV/cn_I [b]	$\delta(ESV/cn_I)$ [c]
Ca^{2+}	Cs^+	Cs^+	Cs^+
Sr^{2+}	K^+	Rb^+	Rb^+
Ba^{2+}	Rb^+	K^+	K^+
K^+	I^-	I^-	Br^-
Rb^+	Br^-	Br^-	Ca^{2+}
Cs^+	Ba^{2+}	Ba^{2+}	Sr^{2+}
Br^-	Sr^{2+}	Sr^{2+}	Ba^{2+}
I^-	Ca^{2+}	Ca^{2+}	I^-

[a] From results at 1 atm. The same order is followed by variations of $\langle\alpha\rangle_I$ and cn_I under the increasing of P.

[b] From results at 1 atm

[c] $\delta(ESV/cn_I) = (ESV/cn_I)(8000atm)$ - $(ESV/cn_I)(1atm)$

5. Acknowledgments

The authors thank the University of Pisa for financial support within the project *PRA_2018_36* "Chirality in Chemistry: a holistic approach".

Appendix A. Supplementary data

References

[1] Y. Marcus, Effect of ions on the structure of water: Structure making and breaking, Chem. Rev. 109 (2009) 1346–1370.

[2] F. J. Millero, The molal volumes of electrolytes approach, Chem. Revs. 71 (1971) 147–176.

[3] V. Mazzini, V. S. J. Craig, What is the fundamental ion-specific series for anions and cations? Ion specificity in standard partial molar volumes of electrolytes and electrostriction in water and non-aqueous solvents, Chem. Sci. 8 (2017) 7052–7065.

[4] N. Galamba, On the effects of temperature, pressure, and dissolved salts on the hydrogen-bond network of water, J. Phys. Chem. B 117 (2013) 589–601.

[5] G. Hummer, S. Garde, A. E. Garcia, A. Pohorille, L. R. Pratt, The pressure dependence of hydrophobic interactions is consistent with the observed pressure denaturation of proteins, Proc. Natl. Acad. Sci. USA 95 (1998) 1552–1555.

[6] T. V. Chalikian, R. B. M. jr, Origins of pressure-induced protein transitions., J. Mol. Biol. 394 (2009) 834–842.

[7] A. Ben-Naim, Theoretical aspects of pressure and solute denaturation of proteins: A kirkwood-buff-theory approach, J. Chem. Phys. 137 (2012) 235102–235110.

[8] B. Meng, H. S. Ashbaugh, Effect of hydrostatic pressure on gas solubilization in micelles, Langmuir 31 (2015) 3318–3325.

[9] F. M. Floris, The formation of a cavity in water: changes of water distribution and prediction of the excess chemical potential of a hard-sphere solute under increasing pressure, J. Molecular Liquids 218 (2016) 166–173.

[10] A. Filipponi, S. D. Panfilis, C. Oliva, M. A. Ricci, P. D'Angelo, D. T. Brown, Ion hydration under pressure, Phys. Rev. Lett. 91 (2003) 165505–165509.

[11] M. Druchok, M. Holovko, Ion hydration under pressure: A molecular dynamics study, J. Mol. Liq. 159 (2011) 24–30.

[12] V. Migliorati, G. Mancini, S. Tatoli, A. Zitolo, A. Filipponi, S. D. Panfilis, A. D. Cicco, P. D'Angelo, Hydration properties of the Zn (2+) ion in water at high pressure, Inorg. Chem. 52 (2013) 1141–1150.

[13] M. Druchok, M. Holovko, Ion hydration under pressure: A molecular dynamics study, Z. Naturforsch. 68a (2013) 112–122.

[14] S. Varma, S. B. Rempe, Coordination numbers of alkali metal ions in aqueous solutions, Bioph. Chem. 124 (2007) 192–199.

[15] F. M. Floris, Nonideal effects on the excess volume from small to large cavities in tip4p water., J. Phys. Chem. B 108 (2004) 16244.

[16] W. Jorgensen, J. Chandrasekhar, J. Madura, R. Impey, M. Klein, Comparison of simple potential functions for simulating liquid water, J. Chem. Phys. 79 (1983) 926.

[17] W. L. Jorgensen, Biochemical and Organic Simulation System (BOSS) Software, Version 4.9, Yale University, New Haven, CT (2013).

[18] K. P. Jensen, W. Jorgensen, Halide, ammonium, and alkali metal ion parameters for modeling aqueous solutions, J. Chem. Theory Comput. 2 (2006) 1499–1506.

[19] J. Aqvist, Ion-water interaction potentials derived from free energy perturbation simuations, J. Phys. Chem. 94 (1990) 8021–8024.

[20] J. Kirkwood, F. Buff, The statistical mechanical theory of solutions., J. Chem. Phys. 19 (1951) 774–777.

[21] N. Matubayasi, R. M. Levy, Thermodynamics of the hydration shell. 2. excess volume and compressibility of a hydrophobic solute., J. Phys.Chem. B 100 (1996) 2681.

[22] T. Lazaridis, Inhomogenous fluid approach to solvation thermodynamics. 1. theory, J. Phys. Chem. B 102 (1998) 3531–3541.

[23] H. Ohtaki, T. Radnai, Structure and dynamics of hydrated ions, Chem. Rev. 93 (1993) 1157–1204.

[24] F. M. Floris, M. Persico, A. Tani, J. Tomasi, Hydration shell structure of the calcium ion from simulations with ab initio effective pair potentials, Chem. Phys. Lett. 227 (1994) 126–132.

[25] T. Ikeda, M. Boero, Communication: Hydration structure and polarization of heavy alkali ions: A first principles molecular dynamics study of Rb(+) and Cs(+), J. Chem. Phys. 137 (2012) 041101–041104.

[26] J. Padova, Ion-solvent interaction. ii. partial molar volume and electrostriction: a thermodynamic approach, J. Chem. Phys. 218 (1963) 1552–1557.